

Theoretical analysis on the origin of the double-well band dispersion in the CuO double chains of $\text{Pr}_2\text{Ba}_4\text{Cu}_7\text{O}_{15-\delta}$ and its impact on superconductivity

Toshiki Yagi,¹ Masayuki Ochi,^{1,2} and Kazuhiko Kuroki¹

¹*Department of Physics, Osaka University, Machikaneyama-cho, Toyonaka, Osaka 560-0043, Japan*

²*Forefront Research Center, Osaka University, Machikaneyama-cho, Toyonaka, Osaka 560-0043, Japan*

(Dated: July 25, 2024)

$\text{Pr}_2\text{Ba}_4\text{Cu}_7\text{O}_{15-\delta}$ is a unique member of cuprate superconductors where many studies suggest that CuO double chains are responsible for superconductivity. One characteristic and non-trivial feature of its electronic structure is a relatively large electron hopping t between nearest neighbor Cu sites with a Cu-O-Cu angle of around 90 degrees. In this study, we have theoretically pinned down the origin of a large $|t|$ in the double-chain structure of $\text{Pr}_2\text{Ba}_4\text{Cu}_7\text{O}_{15-\delta}$ using first-principles calculation and tight-binding-model analysis. We have found that, in the nearest neighbor hopping t , $d-d$ and $d-p-p-d$ contributions roughly cancel each other out and the $d-p-d$ hopping path enhanced by the local distortion of the double chain is a key to get the large $|t|$. Double-well band dispersion arising from the relatively large $|t/t'|$ allows the enhancement of spin-fluctuation-mediated superconductivity by the incipient-band mechanism, where the one band bottom plays a role of the incipient valley. Our study provides the important knowledge to understand the unique superconductivity in $\text{Pr}_2\text{Ba}_4\text{Cu}_7\text{O}_{15-\delta}$.

I. INTRODUCTION

The well-known high T_c family of the cuprate superconductors takes various crystal structures, but most of the family members possess CuO_2 planes playing the main role in the occurrence of superconductivity. Nonetheless, there are some exceptions: a well known example is $(\text{Sr,Ca})_{14}\text{Cu}_{24}\text{O}_{41}$ ¹, in which superconductivity, under pressure, originates from the ladder-like structure within the compound. Another example is $\text{Ae}_2\text{CuO}_{3+\delta}$ ($\text{Ae} = \text{Sr}^2, \text{Ba}^3$), for which the crystal structure is yet to be determined completely. Yet another example is $\text{Pr}_2\text{Ba}_4\text{Cu}_7\text{O}_{15-\delta}$ with T_c ranging from 15 to 30 K⁴⁻⁸. This material consists of an alternating stack of $\text{PrBa}_2\text{Cu}_3\text{O}_{7-\delta}$, which consists of CuO_2 planes and CuO single chains with oxygen deficiencies, and $\text{PrBa}_2\text{Cu}_4\text{O}_8$ composed of CuO_2 planes and CuO double chains, where a number of studies suggest that the double chains are responsible for superconductivity. Experimentally, a Cu nuclear quadrupole resonance (NQR) study have shown that the reduction of $1/T_1T$ is seen below T_c at the double chain sites⁷, suggesting the opening of the superconducting gap at those sites. More recently, a Cu NQR study on a sample exhibiting 100% superconducting volume fraction have shown that the CuO_2 planes are insulating and undergoes antiferromagnetic ordering at low temperatures⁸.

Theoretically, various authors have studied the possibility of unconventional superconductivity taking place in the double chain structure⁹⁻¹⁶. From a tight-binding point of view, much focus has been paid on the electron hopping t between nearest neighbor Cu sites, which reside on different chains among the double-chain structure (see Fig. 1(d)). This type of electron hopping is generally much smaller compared to the next nearest neighbor hopping t' within the chains because the Cu-O-Cu path in the former forms an angle of ~ 90 degrees, while the angle

is ~ 180 degrees in the latter. The effect of finite $|t/t'|$ on the band structure can be understood more easily by unfolding the Brillouin zone (i.e. by taking a reduced unit cell that contains one Cu site), which results in a single band with a double-well structure. Hence, for some range of the band filling, there exist four Fermi points. Considering the Hubbard model with such a band structure from a weak coupling viewpoint, in which only the band structure around the Fermi level matters, the system can be considered as equivalent to a two-leg Hubbard ladder system, which also exhibits four Fermi points^{17,18}, and is known to exhibit superconductivity. Such an effect is obviously absent for $t = 0$, where the double-well structure of the band is lost (in the original double-chain structure, the interchain coupling is lost), so that the effect is naturally expected to be weak when $|t/t'| \ll 1$. Quite recently, this problem has been addressed from a strong coupling point of view, where a one-dimensional t - J model with nearest neighbor J and next nearest neighbor J' were investigated using density matrix renormalization group technique¹⁶. There also, antiferromagnetic nearest neighbor J , which can be considered as originating from t in the strong on-site U limit, is required for the occurrence of superconductivity. In fact, our analysis in the present study shows that $|t/t'|$ is relatively large in $\text{Pr}_2\text{Ba}_4\text{Cu}_7\text{O}_{15}$, compared to, e.g., a well-known two-leg ladder cuprate SrCu_2O_3 , where the two neighboring chains of adjacent ladders form a similar lattice structure as in the double chains of $\text{Pr}_2\text{Ba}_4\text{Cu}_7\text{O}_{15}$. The origin of the relatively large $|t/t'|$ in $\text{Pr}_2\text{Ba}_4\text{Cu}_7\text{O}_{15}$ is thoroughly investigated in the present study, where we find that a local distortion of the crystal structure plays an important role.

Speaking of superconductivity in the two-leg Hubbard ladder, the impact of incipient bands has been studied extensively in the past¹⁹⁻²³. Namely, when the Fermi level intersects one of the bands (say, the bonding band), but barely touches the other (the antibonding band),

TABLE I: Lattice parameters used in this study, which were extracted from experimental studies.

	a (Å)	b (Å)	c (Å)	space group	Ref.
SrCu ₂ O ₃	3.9313	11.5629	3.4926	<i>Cmmm</i>	[31]
PrBa ₂ Cu ₄ O ₈	3.8837	3.90269	27.293	<i>Ammm</i>	[30]
Pr ₂ Ba ₄ Cu ₇ O ₁₅	3.89	3.91	50.74	<i>Ammm</i>	[8]

namely, when the antibonding band is incipient, superconductivity is found to be strongly enhanced. Therefore, one may also expect such an effect to take place in the double-chain system, where “incipient” in this case means that, in the unfolded Brillouin zone, the Fermi level is located near, say, the local minimum of the band. To our knowledge, the band structure and the mechanism of superconductivity in Pr₂Ba₄Cu₇O_{15- δ} have not been analyzed from the viewpoint of incipient bands. In the present study, using fluctuation exchange (FLEX) approximation, we indeed find that superconductivity can be strongly enhanced owing to the incipient band effect.

The paper is organized as follows. Theoretical methods used in this study are described in Sec. II. Sections III A and III B present first-principles and tight-binding analysis on the origin of a sizable $|t/t'|$ in Pr₂Ba₄Cu₇O₁₅. After that, we show our FLEX analysis on the possible superconducting mechanism originating from a large $|t/t'|$ in Sec. III C. Section IV summarizes this study.

II. METHODS

For density functional theory (DFT) calculations, we used the projector augmented wave (PAW) method²⁴ and the Perdew-Burke-Ernzerhof parameterization of the generalized gradient approximation²⁵ as implemented in the Vienna *ab initio* simulation package²⁶⁻²⁹. Core-electron states in PAW potentials were [Kr]4d¹⁰4f², [Kr]4d¹⁰, [Ar]3d¹⁰, [Ar], and [He] for Pr, Ba, Sr, Cu, and O, respectively. Open-core treatment was applied to represent the Pr³⁺ state. We used a plane-wave cutoff energy of 520 eV for Kohn-Sham orbitals without including the spin-orbit coupling for simplicity. A $10 \times 10 \times 10$ \mathbf{k} -mesh was used for all DFT calculations.

We performed structural optimization until the Hellmann-Feynman force becomes less than 0.01 eV \AA^{-1} for each atom. For this purpose, we only optimized atomic coordinates while fixing lattice constants extracted from experiments, which are listed on Table I. For Pr₂Ba₄Cu₇O₁₅, we ignored the partial occupation of oxygen atomic sites representing randomness of the alignment direction of the single-chain structure, and assumed that the single chain aligns along the a direction as the double chain does. We also ignored the oxygen vacancy observed in experiments since its theoretical treatment is difficult.

After DFT calculations, we extracted Wannier orbitals using Wannier90 software³²⁻³⁴. To construct a $d_{x^2-y^2}$ model, we extracted all Cu- $d_{x^2-y^2}$ orbitals in the cell

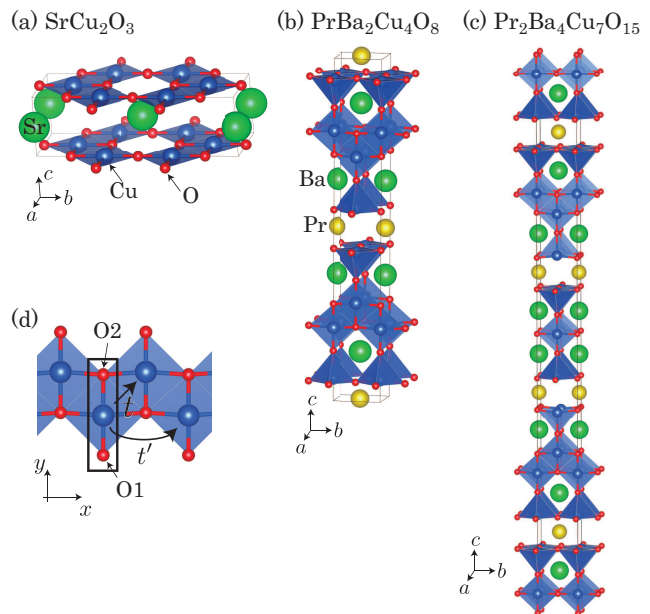


FIG. 1: Crystal structures of (a) SrCu₂O₃, (b) Pr₂Ba₄Cu₇O₁₅, and (c) PrBa₂Cu₄O₈. (d) CuO₂ double-chain structure commonly existing in these three compounds. The nearest neighbor Cu-Cu hopping t and the next nearest neighbor Cu-Cu hopping t' are shown in (d). A black solid square shows the unit cell used in model calculations, where a neighboring unit cell can be represented with a glide reflection. Depicted using the VESTA software³⁷.

and Cu- $d_{3z^2-r^2}$ orbitals on the CuO₂ plane adjacent to the double chain to better reproduce the first-principles band structure. To construct a dp model, we extracted all Cu- d and O- p orbitals in the cell.

To discuss superconductivity, we used a single-orbital Hubbard model,

$$H = \sum_{i,j,\sigma} t_{ij} c_{i,\sigma}^\dagger c_{j,\sigma} + U \sum_i n_{i,\uparrow} n_{i,\downarrow}, \quad (1)$$

where i (j), σ , t , and U denote a site in the unit cell, spin, hopping, and onsite Coulomb interaction, respectively, and analyzed it within FLEX approximation^{35,36}. Using the self energy calculated within FLEX where ring and ladder diagrams are considered, the linearized Eliashberg equation reads

$$\begin{aligned} \lambda \Delta(\mathbf{k}, i\omega_n) &= -\frac{T}{N} \sum_{\mathbf{k}', n'} \Gamma(\mathbf{k} - \mathbf{k}', i(\omega_n - \omega_{n'})) \\ &\times G(\mathbf{k}', i\omega_{n'}) \Delta(\mathbf{k}', i\omega_{n'}) G(-\mathbf{k}', -i\omega_{n'}), \end{aligned} \quad (2)$$

where T , N , Δ , Γ , G , λ are the absolute temperature, the number of cells, the gap function, the pairing interaction, the renormalized Green's function, and the eigenvalue of the linearized Eliashberg equation, respectively. We solved this equation to get λ at a fixed temperature, which we regard as a quantity representing how high the superconducting critical temperature T_c of the system is.

TABLE II: Extracted hopping parameters (in eV) for the $d_{x^2-y^2}$ model.

	t	t'	$ t/t' $
SrCu ₂ O ₃	0.030	-0.480	0.06
PrBa ₂ Cu ₄ O ₈	0.120	-0.521	0.23
Pr ₂ Ba ₄ Cu ₇ O ₁₅	0.117	-0.522	0.22

III. RESULTS AND DISCUSSIONS

A. DFT band structure and hopping parameters

Figure 2 presents DFT band structures together with tight-binding band dispersions obtained by Wannierization. Our tight-binding model well reproduces the original DFT band structure near the Fermi energy. Extracted hopping parameters for the $d_{x^2-y^2}$ model are shown in Table II.

It is noteworthy that $|t/t'|$ largely varies among these three materials: $|t/t'| = 0.06, 0.23,$ and 0.22 for SrCu₂O₃, PrBa₂Cu₄O₈, and Pr₂Ba₄Cu₇O₁₅, respectively. Considering the symmetry of atomic orbitals, it is rather natural to expect $t \sim 0$ as schematically depicted in Fig. 3. As presented in Fig. 3(b), $d_{x^2-y^2}-p_y$ hopping along the x axis is prohibited when $+y$ and $-y$ are equivalent for each atom, i.e., when the parity of $y \rightarrow -y$ can be locally defined. While this symmetry does not rigorously hold in a double-chain structure, it is surprising to get a sizable $|t/t'|$ for PrBa₂Cu₄O₈ and Pr₂Ba₄Cu₇O₁₅.

In the following section, we investigate why such a large $|t/t'|$ is realized in these materials. Since the hopping parameters are similar between these two compounds, we shall focus on Pr₂Ba₄Cu₇O₁₅. We note that similar hopping parameters between PrBa₂Cu₄O₈ and Pr₂Ba₄Cu₇O₁₅ suggest that the absence of superconductivity in the former compound is not due to a change in the band structure. In fact, some researchers pointed out that the absence of superconductivity in PrBa₂Cu₄O₈ might be due to a difference in the carrier density, which can be controlled in Pr₂Ba₄Cu₇O₁₅ through the oxygen deficiency in CuO single chains⁵.

B. Origin of the sizable $|t/t'|$: analysis on the dp model

1. Model simplification

To investigate the origin of the sizable $|t/t'|$ in Pr₂Ba₄Cu₇O₁₅, we analyzed the dp models for SrCu₂O₃ and Pr₂Ba₄Cu₇O₁₅ and compared them. Since the dp model consists of all Cu- d and O- p orbitals in the cell, we first eliminated irrelevant orbitals from the model in the following way.

Figure 4 presents band dispersion for the full dp model and that for the ‘isolated double-chain’ dp model of Pr₂Ba₄Cu₇O₁₅. Here, the latter model was constructed by extracting Cu- $d_{x^2-y^2}$ and O- $p_{x,y}$ orbitals inside the

TABLE III: All possible combinations of the orbitals for the isolated double-chain model without O1- p_x . Note that Cu- $d_{x^2-y^2}$ orbital is already taken because our purpose is to evaluate an effective hopping value t between Cu- $d_{x^2-y^2}$.

	Cu- $d_{x^2-y^2}$	O1- p_y	O2- p_x	O2- p_y
model 1	✓			
model 2	✓	✓		
model 3	✓		✓	
model 4	✓	✓	✓	
model 5	✓			✓
model 6	✓	✓		✓
model 7	✓		✓	✓
model 8	✓	✓	✓	✓

double chain (i.e., Cu- $d_{x^2-y^2}$ and O- $p_{x,y}$ orbitals defined on the atom sites shown in Fig. 1(d)) from the full dp model. Inter-double-chain hoppings were also eliminated, by which we call it the ‘isolated’ double chain. Since the band dispersion of the double chain is well reproduced by the isolated double-chain model, we focus on the latter model hereafter.

From here on, we consider a halved unit cell as shown in Fig. 1(d), where O1- $p_{x,y}$, O2- $p_{x,y}$, and Cu- $d_{x^2-y^2}$ orbitals are included in the unit cell. A neighboring unit cell is obtained by glide reflection of the cell (i.e., translation in addition to the $y \rightarrow -y$ reflection). Thus, while this cannot be considered as a unit cell in first-principles calculations, this reduced cell can be regarded as a unit cell in model calculations. A similar model construction was applied to iron-based superconductors having non-symmorphic symmetry³⁸.

We applied further simplification to the model. Since we found that O1- p_x has a negligible effect on the topmost $d_{x^2-y^2}$ band as shown in Fig. 5, we also excluded O1- p_x from the model in the following analysis. Note that the model has a single d band in the folded Brillouin zone by halving the unit cell.

2. Analysis of $|t/t'|$

To theoretically pin down important hopping paths in the isolated double-chain dp model, we evaluated how the effective value of t changes when the model consists of a subset of orbitals. We tried all possible combinations of the orbitals within the isolated double-chain model without O1- p_x , as listed in Table III, and extracted the hopping parameters t and t' by performing Fourier transformation for the topmost $d_{x^2-y^2}$ band for each model. Namely, considering the one-dimensional structure without inter-double-chain hoppings, the topmost $d_{x^2-y^2}$ band dispersion can be expanded as

$$\epsilon(k_x) = 2t \cos k_x + 2t' \cos(2k_x) + 2t'' \cos(3k_x) + \dots, \quad (3)$$

where the coefficient of each term obtained by Fourier transform can be regarded as the effective hoppings for the $d_{x^2-y^2}$ model.

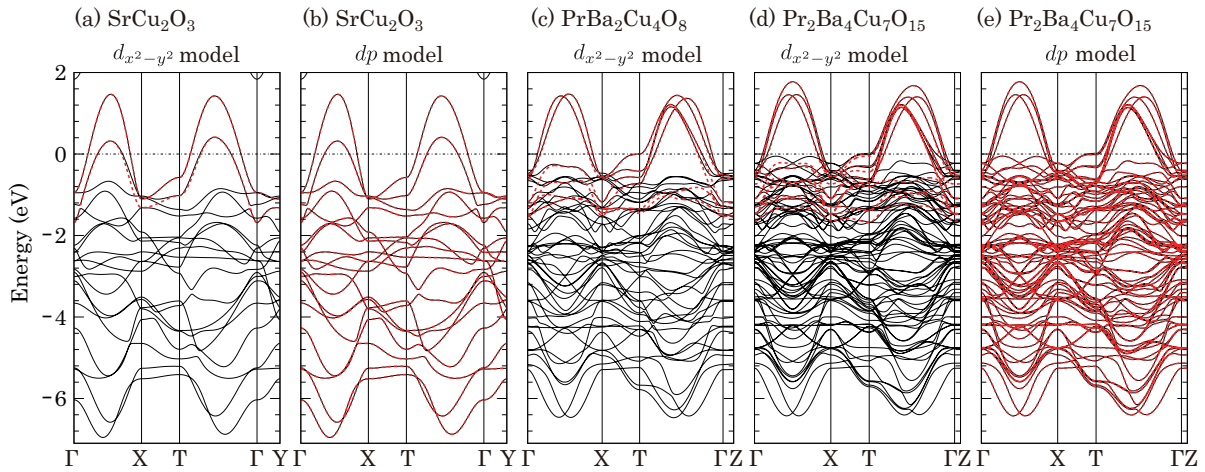


FIG. 2: Electronic band structures of (a)(b) SrCu_2O_3 , (c) $\text{PrBa}_2\text{Cu}_4\text{O}_8$, and (d)(e) $\text{Pr}_2\text{Ba}_4\text{Cu}_7\text{O}_{15}$. First-principles band structure and that for the tight-binding model extracted by Wannierization are shown with black solid lines and red broken lines, respectively. The $d_{x^2-y^2}$ and dp models are shown for (a)(c)(d) and (b)(e), respectively. The band dispersion was depicted along $\Gamma(0,0,0) - X(2\pi/a,0,0) - T(2\pi/a,0,2\pi/c) - \Gamma - Y(0,2\pi/b,0)$ for SrCu_2O_3 and $\Gamma(0,0,0) - X(2\pi/a,0,0) - T(2\pi/a,2\pi/b,0) - \Gamma - Z(0,0,2\pi/c)$ for $\text{Pr}_2\text{Ba}_4\text{Cu}_7\text{O}_{15}$ and $\text{PrBa}_2\text{Cu}_4\text{O}_8$ (in the cartesian coordinate).

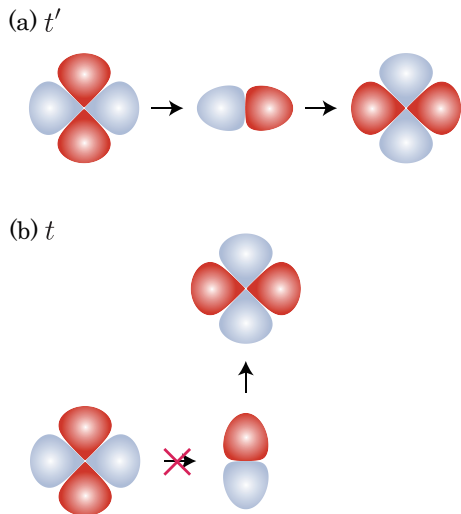


FIG. 3: Hopping processes (a) t' and (b) t between $\text{Cu}-d_{x^2-y^2}$ orbitals via an $\text{O}-p$ orbital in a double chain.

Figure 6(a) presents an extracted value of t for each model, where the model index is defined in Table III. We found that the extracted values of t are roughly consistent between SrCu_2O_3 and $\text{Pr}_2\text{Ba}_4\text{Cu}_7\text{O}_{15}$ for models 1–4, but this is not the case for models 5–8. Since model 5–8 contains $\text{O}2-p_y$ while it is not included in models 1–4, this result suggests that a main cause of the difference in t between two materials is brought by $\text{O}2-p_y$.

To get further insight into the role of $\text{O}2-p_y$, in Fig. 6(b), we present t evaluated for these models without including a specific hopping, $t[d-p_y;\text{O}2]$, which is defined in Fig. 6(c). This is the nearest neighbor hopping between $\text{Cu}-d_{x^2-y^2}$ and $\text{O}2-p_y$ along the x direction, which is prohibited when the $y \rightarrow -y$ symmetry exists for each

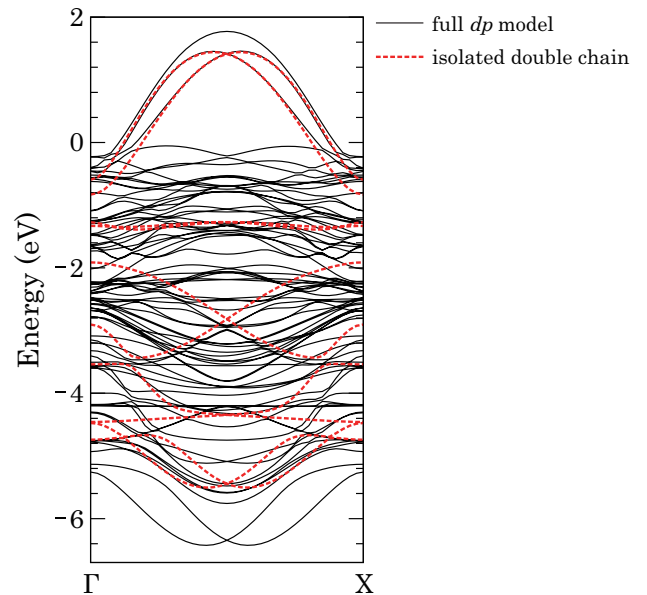


FIG. 4: Band dispersion for the tight-binding model of $\text{Pr}_2\text{Ba}_4\text{Cu}_7\text{O}_{15}$. Black solid and red broken lines present the band dispersion for the full dp model and that for the ‘isolated double-chain’ dp model as defined in the main text, respectively. For the latter model, the band dispersion is slightly ($+0.14$ eV) shifted.

atomic site and then $d_{x^2-y^2}$ and p_y have even and odd parities, respectively. In fact, $t[d-p_y;\text{O}2]$ in SrCu_2O_3 is small, 0.093 eV, even though the perfect $y \rightarrow -y$ symmetry no longer exists. On the other hand, we found that $\text{Pr}_2\text{Ba}_4\text{Cu}_7\text{O}_{15}$ has a sizable $t[d-p_y;\text{O}2] = 0.204$ eV. Since this hopping is expected to largely contribute to the t hopping path, the size of $t[d-p_y;\text{O}2]$ can be the main ori-

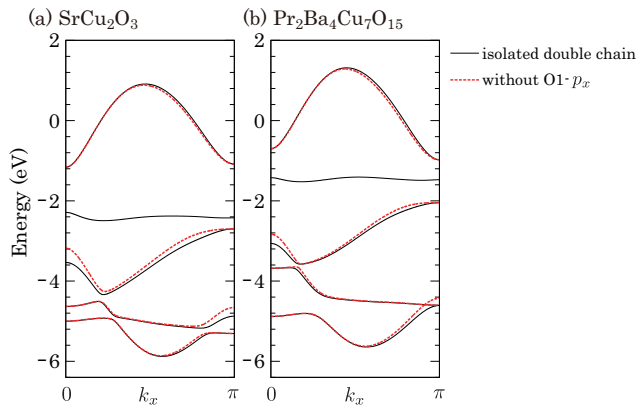


FIG. 5: Band dispersion for the tight-binding model of (a) SrCu_2O_3 and (b) $\text{Pr}_2\text{Ba}_4\text{Cu}_7\text{O}_{15}$. Black solid and red broken lines present the band dispersion for the ‘isolated double-chain’ dp model and that without the O1- p_x orbital, respectively.

gin of different t between SrCu_2O_3 and $\text{Pr}_2\text{Ba}_4\text{Cu}_7\text{O}_{15}$; this expectation is verified in Fig. 6(b), where the difference between the two materials is drastically decreased compared with Fig. 6(a) by hypothetically excluding $t[d - p_{y;\text{O}2}]$ from the models.

We note that, while the main difference in t between SrCu_2O_3 and $\text{Pr}_2\text{Ba}_4\text{Cu}_7\text{O}_{15}$ is due to the size of $t[d - p_{y;\text{O}2}]$, there are many other relevant hopping paths contributing to t . In fact, the value of t largely varies among different models in Fig. 6(b). For example, a d - p - p - d hopping path shown in Fig. 6(d) can contribute to t , which is included in models 3, 4, 7, and 8, where O2- p_x is included. Another d - p - p - d path shown in Fig. 6(e) is included in models 6 and 8, where both O1- p_y and O2- p_y are included. In Fig. 6(b), it seems that t is increased by these hopping paths. As we have seen in the previous paragraph, t is also increased by the hopping path using $t[d - p_{y;\text{O}2}]$, which is most likely d - p - d . On the other hand, the negative t value for the model 1, where no oxygen orbitals are included, is the direct d - d hopping.

To summarize, the direct d - d hopping gives a negative $t \sim -0.2$ eV (see model 1 in Fig. 6(a) or (b)) while the d - p - p - d (or longer) hopping paths via oxygen p -orbitals raise the value of t . Although these two contributions are roughly canceled out (see model 8 in Fig. 6(b)), the d - p - d hopping path with a large $t[d - p_{y;\text{O}2}]$ results in a positive and sizable t for $\text{Pr}_2\text{Ba}_4\text{Cu}_7\text{O}_{15}$ (see model 8 in Figs. 6(a)).

To investigate the reason for the sizable $t[d - p_{y;\text{O}2}]$ in $\text{Pr}_2\text{Ba}_4\text{Cu}_7\text{O}_{15}$, we checked how the local structure of Cu-O double chains affects the hopping parameters. For this purpose, we hypothetically changed the O2 coordinate along the y direction for SrCu_2O_3 and extracted t and $t[d - p_{y;\text{O}2}]$ for each structure. The results are shown in Fig. 7. Note that these t values were simply extracted by Wannierization for the $d_{x^2-y^2}$ model. This plot clearly shows that both t and $t[d - p_{y;\text{O}2}]$ are sizably increased when the O-Cu-O angle moves away from 180° . There-

TABLE IV: Hopping parameters (eV) used in Fig. 8, which were extracted by first-principles calculation and Wannier construction of the $d_{x^2-y^2}$ model.

t	t'	t''	t'''	t''''	t_z	t'_z	t''_z
0.117	-0.522	-0.041	-0.069	-0.012	-0.013	-0.014	-0.014

fore, a somewhat large discrepancy from 180° in the O-Cu-O angle for $\text{Pr}_2\text{Ba}_4\text{Cu}_7\text{O}_{15}$ seems to be important to understand the large $t[d - p_{y;\text{O}2}]$ and therefore t in this compound.

C. Superconductivity in the double chain

We have investigated the origin of large $|t/t'|$ in $\text{Pr}_2\text{Ba}_4\text{Cu}_7\text{O}_{15}$. In this section, we see how this aspect is related to the superconductivity in this compound. For this purpose, we constructed a single-orbital Hubbard model consisting of the Cu- $d_{x^2-y^2}$ orbital on the double chain. We extracted hopping parameters from the $d_{x^2-y^2}$ model as described before, and the parameters considered in the following analysis are shown in Table IV. Here, the unit cell in model calculation is shown in Fig. 8(a), which contains a single Cu site. Inter-double-chain hopping along the z direction (the a direction in the original lattice) was considered.

Then, we performed FLEX + Eliashberg calculation using $U = 2.5$ eV as a typical value of cuprates, the temperature $T = 5$ and 7.5 meV, a 256×16 \mathbf{k} -mesh, and 2×2048 Matsubara frequencies. The obtained eigenvalue of the linearized Eliashberg equation λ and the Stoner factor $\alpha = \max_{\mathbf{q}}[U\chi_0(\mathbf{q}, 0)]$, where χ_0 is the irreducible susceptibility at the lowest (Bosonic) Matsubara frequency in FLEX, are shown in Figs. 8(b) and (c), respectively. We note that it is difficult to theoretically determine the band filling n for the double chain. One reason for it is that a charge transfer among the CuO_2 plane, the double chain, and the single chain should occur in the actual material where the CuO_2 plane is a Mott insulator^{4,5,8}. Another reason is that the actual material has oxygen vacancy^{4,5}. Thus, in this study, we set n as a variable and plotted λ and α as a function of n . We excluded data points near the half filling $n = 0.5$ since the strong electron correlation effects near the half filling is difficult to describe for the weak-coupling theory such as FLEX.

We can see a notable peak of λ around $n \sim 0.1$ in Fig. 8(b), which was not discussed in the previous FLEX study¹⁰. It is also noteworthy that the Stoner factor α is less than 0.85 at the peak of λ , which is rather small for such a large λ in FLEX + Eliashberg calculations. Such a small α indicates that the system is far from magnetic ordering, and suggests that a main glue of superconductivity is not a zero-energy spin fluctuation on the Fermi surface. Figure 8(d) presents the gap function $\Delta(\mathbf{k}, i\omega_0)$ at the lowest (Fermion) Matsubara frequency $\omega_0 = i\pi k_B T$ (bottom) shown together with

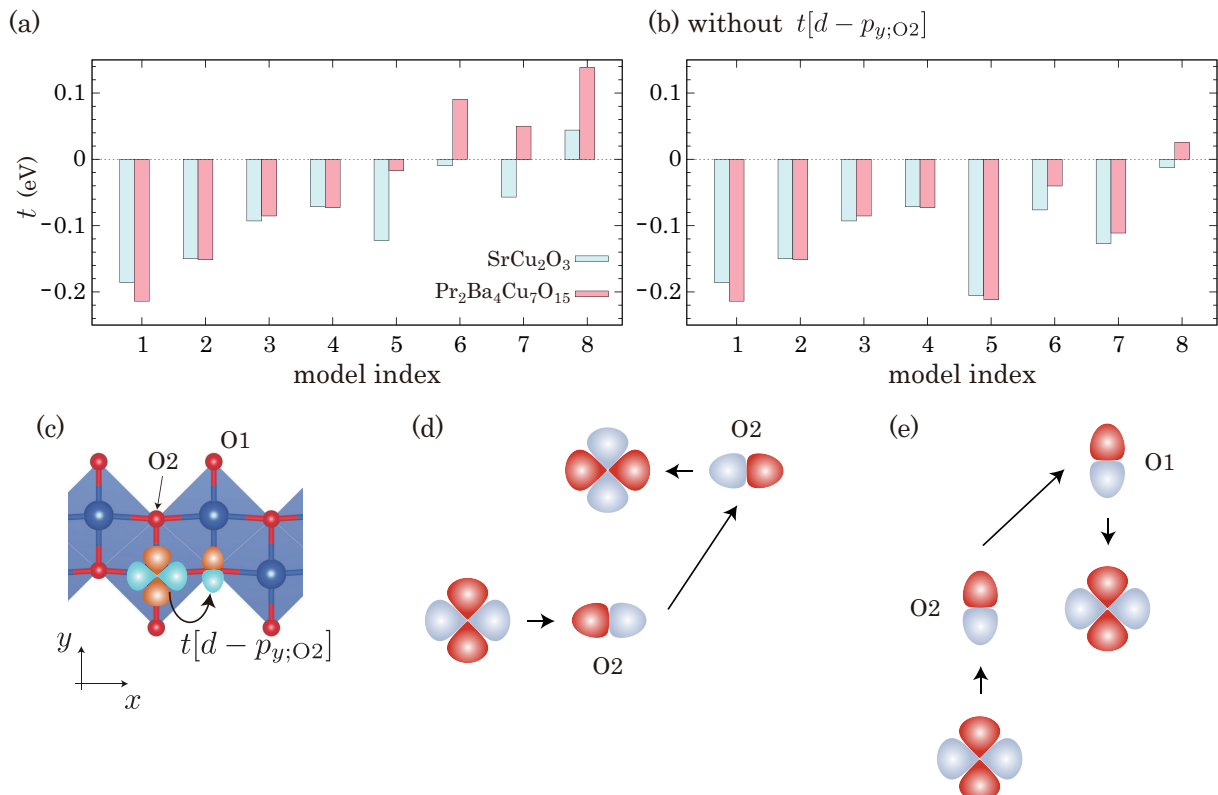


FIG. 6: (a) Extracted t values for models defined in Table III for SrCu₂O₃ and Pr₂Ba₄Cu₇O₁₅. (b) Those evaluated by hypothetically excluding $t[d - p_y; O_2]$ from the models. (c) Definition of $t[d - p_y; O_2]$. (d)(e) Possible d - p - p - d hopping paths contributing to t .

the tight-binding band dispersion (top) for $T = 5$ meV, $n = 0.103$, where λ has a peak. Broken black lines in the bottom panel presents the Fermi surface of the renormalized band dispersion: $\epsilon^0(\mathbf{k}) + \text{Re}[\Sigma(\mathbf{k}, i\omega_0)]$ where the self-energy correction was added to the non-interacting band dispersion $\epsilon^0(\mathbf{k})$. The gap function shows that the Cooper-pair scattering between $k_x = 0$ and $k_x = \pi$ is a glue of the superconductivity. While the Fermi surface is formed around $k_x = \pi$ irrespective of k_z , only a small pocket exists around the $k_x = 0$ line. Considering the small Stoner factor, the finite-energy spin fluctuation seems to be crucial here. This situation reminds us the incipient-band superconductivity in multi-band systems, where the finite-energy pair scattering between the band intersecting the Fermi level and that lying just near the Fermi level is a key for superconductivity^{19–23}. While our model has a single band, the band dispersion has a double-well structure with different energies for two valleys due to the sizable $|t/t'|$, by which the incipient-band mechanism can be realized.

A key in the superconducting mechanism described above is the double-well structure of the non-interacting band dispersion. To understand this situation more clearly, we also performed FLEX + Eliashberg calculation for a simplified model. In the simplified model, we only considered t , t' , and t_z . The non-interacting band

dispersion reads

$$\epsilon^0(\mathbf{k}) = 2t \cos k_x + 2t' \cos(2k_x) + 2t_z \cos k_z. \quad (4)$$

The role of t is clear: the $2t' \cos(2k_x)$ term makes the double-well band structure with the same energy for $k_x = 0, \pi$ and the $2t \cos k_x$ term makes the energies of $k_x = 0, \pi$ different. We set $t' = -1$ as an energy unit, $t_z/t' = -0.05$, and tried several values of $t/|t'|$ to see the role of t . While t' was taken as an energy unit, we set its sign negative in accord with Table IV. We used $U/|t'| = 5$, $T/|t'| = 0.01$, a 256×16 \mathbf{k} -mesh, and 2×4096 Matsubara frequency. The calculated results for $t/|t'| = 0.1, 0.2, 0.3$ are shown in Fig. 9, where we can see similar peaks to that shown in Fig. 8(b). While the peak of λ can be seen also for a relatively small $t/|t'|$, it is clear that a large $|t/|t'|$ is desirable for superconductivity. The peak position of λ was shifted toward a larger band filling n for a larger $t/|t'|$, which is naturally understood considering the incipient-band mechanism: the band filling where the Fermi level reaches the bottom of the band dispersion at $k_x = 0$ becomes large for a large $t/|t'|$ (see Fig. 8(d)). In fact, we verified that the Fermi level locates around the bottom of the band dispersion at $k_x = 0$ for all $t/|t'|$ when λ reaches its peak.

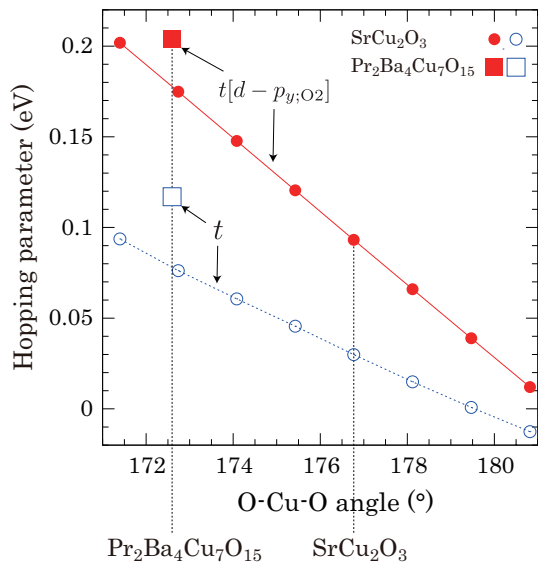


FIG. 7: Extracted t (red filled symbols) and $t[d - p_{y;O2}]$ (blue open symbols) values plotted against the O-Cu-O angle along the x direction in the double chain. Square and circle symbols denote the values for $\text{Pr}_2\text{Ba}_4\text{Cu}_7\text{O}_{15}$ and SrCu_2O_3 , respectively. For SrCu_2O_3 , we hypothetically moved the O2 coordinate along the y direction in calculation to change the O-Cu-O angle. Vertical black broken lines represent the Cu-O-Cu angles obtained by structural optimization for two compounds.

IV. SUMMARY

In this study, we have theoretically pinned down the origin of a large $|t/t'|$ in the double-chain structure of $\text{Pr}_2\text{Ba}_4\text{Cu}_7\text{O}_{15-\delta}$ using first-principles calculation and tight-binding-model analysis. We have found that, in the nearest neighbor hopping t , $d-d$ and $d-p-p-d$ contributions roughly cancel each other out and the $d-p-d$ hopping path enhanced by the local distortion of the double chain is a key to get the large $|t|$. This is in contrast to the small interchain coupling in SrCu_2O_3 , where the local distortion and thus the $d-p-d$ contribution are small. Double-well band dispersion arising from the relatively large $|t/t'|$ allows the enhancement of spin-fluctuation-mediated superconductivity by the incipient-band mechanism, where the one band bottom plays a role of the incipient valley. Our study provides the important knowledge to understand the unique superconductivity in $\text{Pr}_2\text{Ba}_4\text{Cu}_7\text{O}_{15-\delta}$.

Acknowledgments

We thank Dr. Tatsuya Kaneko for fruitful discussions. This study was supported by JSPS KAKENHI Grant No. JP22K04907 and No. JP24K01333. The computing resource was supported by the supercomputer system in the Institute for Solid State Physics, the University of Tokyo.

- ¹ M. Uehara, T. Nagata, J. Akimitsu, H. Takahashi, N. Môri, and K. Kinoshita, J. Phys. Soc. Jpn. **65**, 2764 (1996).
- ² Z. Hiroi, M. Takano, M. Azuma, and Y. Takeda, Nature **364**, 315 (1993).
- ³ W. M. Li, J. F. Zhao, L. P. Cao, Z. Hu, Q. Z. Huang, X. C. Wang, Y. Liu, G. Q. Zhao, J. Zhang, Q. Q. Liu, R. Z. Yu, Y. W. Long, H. Wu, H. J. Lin, C. T. Chen, Z. Li, Z. Z. Gong, Z. Guguchia, J. S. Kim, G. R. Stewart, Y. J. Uemura, S. Uchida, and C. Q. Jin, Proc. Natl. Acad. Sci. U.S.A. **116**, 12156 (2019).
- ⁴ M. Matsukawa, Y. Yamada, M. Chiba a, H. Ogasawara, T. Shibata, A. Matsushita, and Y. Takano, Physica C **411**, 101 (2004).
- ⁵ Y. Yamada and A. Matsushita, Physica C **426**, 213 (2005).
- ⁶ K. Honnami, M. Matsukawa, T. Senzaki, T. Toyama, H. Taniguchi, K. Ui, T. Sasaki, K. Takahashi, M. Hagiwara, Physica C **585**, 1353869 (2021).
- ⁷ S. Watanabe, Y. Yamada, and S. Sasaki, Physica C **426**, 473 (2005).
- ⁸ S. Nishioka, S. Sasaki, S. Nakagawa, M. Yashima, H. Mukuda, M. Yogi, and J. ichi Shimoyama, Appl. Phys. Express **15**, 023001 (2022).
- ⁹ K. Sano, Y. Ôno, and Y. Yamada, J. Phys. Soc. Jpn. **74**, 2885 (2005).
- ¹⁰ T. Nakano, K. Kuroki, and S. Onari, Phys. Rev. B **76**, 014515 (2007).
- ¹¹ K. Sano and Y. Ôno, J. Phys. Soc. Jpn. **76**, 113701 (2007).
- ¹² K. Okunishi, Phys. Rev. B **75**, 174514 (2007).
- ¹³ E. Berg, T. H. Geballe, and S. A. Kivelson, Phys. Rev. B **76**, 214505 (2007).
- ¹⁴ S. Nishimoto, K. Sano, and Y. Ohta, Phys. Rev. B **77**, 085119 (2008).
- ¹⁵ T. Habaguchi, Y. Ôno, H. Ying Du Gh, K. Sano, and Y. Yamada, J. Phys. Soc. Jpn. **80**, 024708 (2011).
- ¹⁶ T. Kaneko, S. Ejima, K. Sugimoto, and K. Kuroki, J. Phys. Soc. Jpn. **93**, 084703 (2024).
- ¹⁷ M. Fabrizio, Phys. Rev. B **54**, 10054 (1996).
- ¹⁸ K. Kuroki, R. Arita, and H. Aoki, J. Phys. Soc. Jpn. **66**, 3371 (1997).
- ¹⁹ K. Kuroki, T. Higashida, and R. Arita, Phys. Rev. B **72**, 212509 (2005).
- ²⁰ K. Matsumoto, D. Ogura, K. Kuroki, Phys. Rev. B **97**, 014516(2018).
- ²¹ K. Matsumoto, D. Ogura, K. Kuroki, J. Phys. Soc. Jpn. **89**, 044709 (2020).
- ²² D. Kato and K. Kuroki, Phys. Rev. Res. **2**, 023156 (2020).
- ²³ H. Sakamoto and K. Kuroki, Phys. Rev. Res. **2**, 022055(R) (2020).
- ²⁴ G. Kresse and D. Joubert, Phys. Rev. B **59**, 1758 (1999).
- ²⁵ J. P. Perdew, K. Burke, and M. Ernzerhof, Phys. Rev. Lett. **77**, 3865 (1996).
- ²⁶ G. Kresse and J. Hafner, Phys. Rev. B **47**, 558 (1993).
- ²⁷ G. Kresse and J. Hafner, Phys. Rev. B **49**, 14251 (1994).
- ²⁸ G. Kresse and J. Furthmüller, Comput. Mater. Sci. **6**, 15

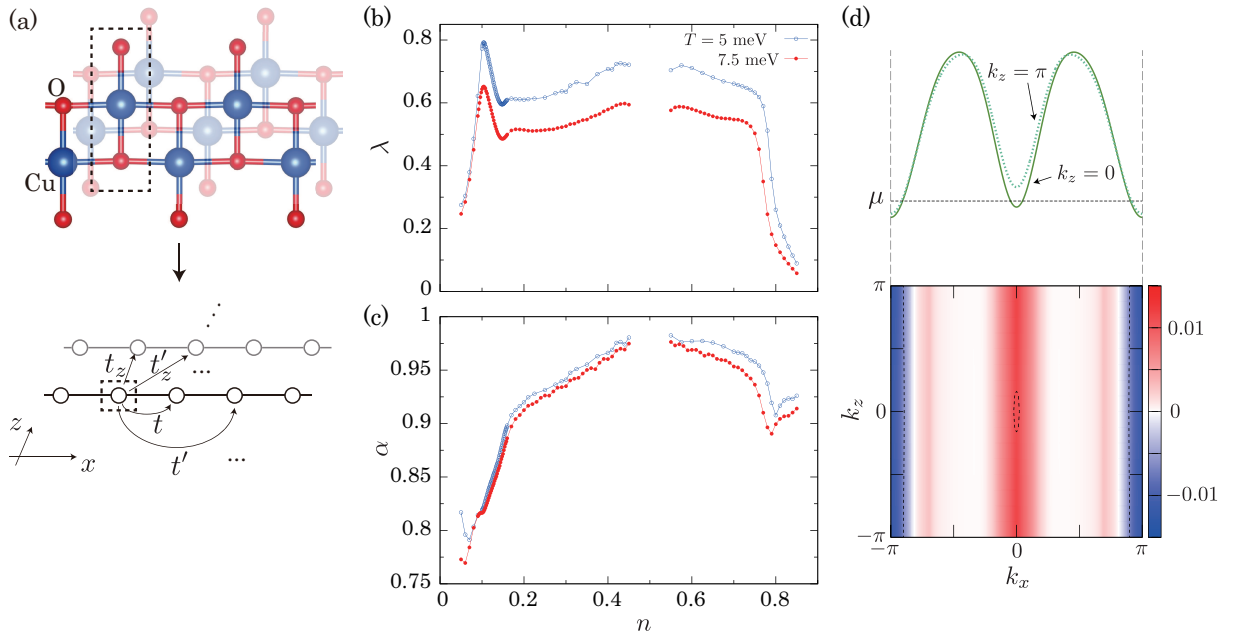


FIG. 8: Calculation results for FLEX + Eliashberg calculations of the Cu- $d_{x^2-y^2}$ model for $\text{Pr}_2\text{Ba}_4\text{Cu}_7\text{O}_{15}$. (a) A unit cell and the definition of hopping parameters, (b) the calculated eigenvalue of the linearized Eliashberg equation λ , (c) the Stoner factor α , and (d) the gap function $\Delta(\mathbf{k}, i\omega_0)$ at the lowest Matsubara frequency $\omega_0 = i\pi k_B T$ (bottom) shown together with the tight-binding band dispersion (top) for $T = 5$ meV, $n = 0.103$, where λ has a peak in (b). Broken black lines in the bottom panel presents the Fermi surface of the renormalized band dispersion (see the main text).

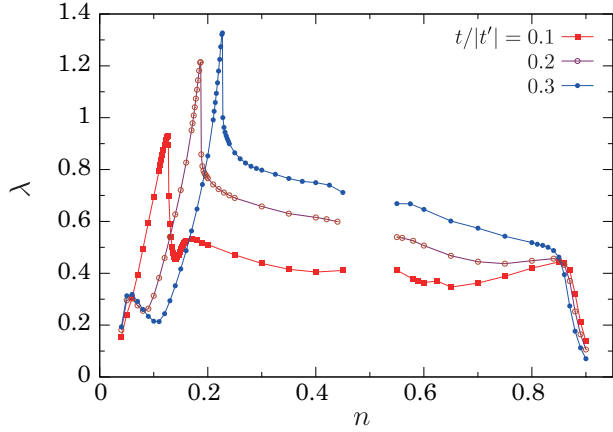


FIG. 9: FLEX + Eliashberg calculation results for a simplified model. The calculated eigenvalue of the linearized Eliashberg equation λ was plotted against the band filling n .

- (1996).
²⁹ G. Kresse and J. Furthmüller, Phys. Rev. B **54**, 11169 (1996).
³⁰ Y. Yamada, J. Ye, S. Horii, A. Matsushita, and S. Kubo, J. Phys. Chem. Solids **62**, 191 (2001).
³¹ M. Azuma, H. Yoshida, T. Saito, T. Yamada, and M. Takano, J. Am. Chem. Soc. **126**, 8244 (2004).
³² N. Marzari and D. Vanderbilt, Phys. Rev. B **56**, 12847 (1997).
³³ I. Souza, N. Marzari, and D. Vanderbilt, Phys. Rev. B **65**, 035109 (2001).
³⁴ G. Pizzi *et al.*, J. Phys.: Condens. Matter **32**, 165902 (2020).
³⁵ N. E. Bickers, D. J. Scalapino, and S. R. White, Phys. Rev. Lett. **62**, 961 (1989).
³⁶ T. Dahm and L. Tewordt, Phys. Rev. Lett. **74**, 793 (1995).
³⁷ K. Momma and F. Izumi, J. Appl. Crystallogr. **44**, 1272 (2011).
³⁸ K. Kuroki, S. Onari, R. Arita, H. Usui, Y. Tanaka, H. Kon-tani, and H. Aoki, Phys. Rev. Lett. **101**, 087004 (2008).